J. Phys. B: At. Mol. Opt. Phys. **28** (1995) 839–856. Printed in the UK

Absolute differential cross sections for electron-impact excitation of CO near threshold: II. The Rydberg states of CO

J Zobel†, U Mayer†, K Jung†, H Ehrhardt†, H Pritchard‡, C Winstead‡ and V McKoy‡

† Fachbereich Physik, Universität Kaiserslautern, D-67663 Kaiserslautern, Germany

‡ A A Noyes Laboratory of Chemical Physics, California Institute of Technology, Pasadena, CA 91125, USA

Received 18 August 1995, in final form 24 November 1995

Abstract. Absolute differential cross sections for electron-impact excitation of Rydberg states of CO have been measured from threshold to 3.7 eV above threshold and for scattering angles between 20° and 140°. Measured excitation functions for the b $^3\Sigma^+$, B $^1\Sigma^+$ and E $^1\Pi$ states are compared with cross sections calculated by the Schwinger multichannel method. The behaviour of the excitation functions for these states and for the j $^3\Sigma^+$ and C $^1\Sigma^+$ states is analysed in terms of negative-ion states. One of these resonances has not been previously reported.

1. Introduction

Absolute differential cross sections for electron-impact excitation of the ground state of the CO molecule into five of the six lowest Rydberg states have been measured in the energy range from threshold to 3.7 eV above threshold and for scattering angles from 20° to 140°. The electronic configurations of these states (b $^3\Sigma^+$, B $^1\Sigma^+$, j $^3\Sigma^+$, C $^1\Sigma^+$ and E $^1\Pi$) are described by Rydberg electrons bound to the X $^2\Sigma^+$ ionic core, with an electron configuration $KL1\pi^4 5\sigma$. In contrast to the long vibrational progressions characteristic of the energy-loss spectra for the valence states of CO, a few vibrationally elastic transitions dominate the spectra for these Rydberg states.

Differential cross sections for the electron-impact excitation of Rydberg states of CO at low detection energies have been measured by several groups. Mazeau *et al* (1972) measured relative differential cross sections for excitation of the b $^3\Sigma^+$ and B $^1\Sigma^+$ states, while Swanson *et al* (1975) have reported excitation cross sections for the b $^3\Sigma^+$, B $^1\Sigma^+$, C $^1\Sigma^+$, c $^3\Pi$ and E $^1\Pi$ states at a single scattering angle (45°). Allan (1989) has also reported relative excitation functions for the b $^3\Sigma^+$, B $^1\Sigma^+$ and j $^3\Sigma^+$ states. Allan's results, obtained using a trochoidal spectrometer, only include contributions from scattering angles near 0° and 180°, which are inaccessible with our apparatus; thus, direct comparison with our results is not possible.

Although most theoretical studies of electronic excitation of CO by low-energy electron impact have focused on the valence states, some work has been reported on the Rydberg states of this molecule. Chung and Lin (1974) used the Ochkur–Rudge approximation to calculate cross sections for the A $^1\Pi$, b $^3\Sigma^+$, B $^1\Sigma^+$, C $^3\Sigma^+$ and E $^1\Pi$ states of CO. References to earlier theoretical studies may be found in their paper. Weatherford and Huo (1990) have reported cross sections for excitation of the b $^3\Sigma^+$ state calculated using the Schwinger multichannel (SMC) method.

0953-4075/95/040839+18$19.50

A description of the experimental apparatus and procedures used in these measurements has been given in paper I in this issue. In the section below, we briefly outline the procedure used to calculate cross sections for some of the transitions studied in this paper. We then present an overview of the resonances we have observed in excitation of Rydberg states of CO. This is followed by a discussion of the measured integral and differential cross sections for excitation of the b $^3\Sigma^+$, B $^1\Sigma^+$, j $^3\Sigma^+$, C $^1\Sigma^+$ and E $^1\Pi$ Rydberg states and a comparison with the results of calculations for the b $^3\Sigma^+$, B $^1\Sigma^+$ and E $^1\Pi$ states.

2. Computational details

Details of the Schwinger multichannel (SMC) method and its implementation on highly parallel computers used in these studies have been given previously (Takatsuka and McKoy 1984 and Winstead *et al* 1991). Here it is sufficient to note that the scattering amplitude is obtained by evaluating the variational expression

$$f(\boldsymbol{k}_m, \boldsymbol{k}_n) = -\frac{1}{2\pi} \sum_{ij} \langle S_m | V | \chi_i \rangle \left(A^{-1}\right)_{ij} \langle \chi_j | V | S_n \rangle \tag{1}$$

where $S_{m(n)} = \Phi_{m(n)} \exp(\mathrm{i}\boldsymbol{k}_{m(n)} \cdot \boldsymbol{r}_{N+1})$ is the product of an eigenstate of the target, $\Phi_{m(n)}$, and a plane wave, V is the interaction potential between the electron and the molecule, and $\chi_{i(j)}$ are configuration state functions of the $(N+1)$-electron system, i.e. spin eigenfunctions formed from determinants of one-electron orbitals. The A_{ij} matrix elements involve projected forms of the interaction potential V, the Hamiltonian of the $(N+1)$-electron system, and a projected free-particle Green function. With an expansion of the one-electron orbitals in the χ_i and Φ_m in a basis of Cartesian Gaussian functions, all matrix elements appearing in equation (1) can be evaluated analytically except those arising from the Green function. We evaluate these terms by numerical quadrature using a procedure that has been efficiently implemented on distributed-memory parallel computers (Hipes *et al* 1990).

The cross sections for the dipole-allowed transitions of interest in this study include long-range, high partial-wave contributions which are difficult to represent in the L^2 expansion of the scattering wavefunction used in our implementation of the SMC method. We include the contribution of these higher partial waves to the scattering amplitudes by means of a Born-closure procedure. In this approximation, the scattering amplitude is given by

$$f^{\mathrm{COM}}(\boldsymbol{k}_{\Gamma'}, \boldsymbol{k}_{\Gamma}) = f^{\mathrm{FBA}}(\boldsymbol{k}_{\Gamma'}, \boldsymbol{k}_{\Gamma}) + \sum_{ll'}^{l_{\max}} \sum_{mm'}^{m_{\max}} \left[f^{\mathrm{SMC}}_{l'm',lm}(k_{\Gamma'}, k_{\Gamma}) - f^{\mathrm{FBA}}_{l'm',lm}(k_{\Gamma'}, k_{\Gamma}) \right] Y_{l'm'}(\hat{k}_{\Gamma'}) Y^*_{lm}(\hat{k}_{\Gamma}) \tag{2}$$

where $f^{\mathrm{FBA}}(\boldsymbol{k}_{\Gamma'}, \boldsymbol{k}_{\Gamma})$ is the first-Born scattering amplitude for the transition (Chung and Lin 1974) and f^{SMC} and f^{COM} are the scattering amplitude of equation (1) and the laboratory-frame scattering amplitude, respectively. We evaluate equation (2) directly in the laboratory frame. Although this requires evaluation of the first-Born amplitude at a large number of quadrature points, the computation can be efficiently decomposed and carried out on parallel computers. This procedure will be discussed in greater detail in a forthcoming publication.

In this study, we used the improved virtual orbital (IVO) method of Hunt and Goddard (1969) to obtain Rydberg orbitals for the b $^3\Sigma^+$, B $^1\Sigma^+$ and E $^1\Pi$ states. The one-particle basis consisted of a [10s6p]/(5s4p) basis (Dunning 1971) augmented with diffuse s, p and

Table 1. Cartesian Gaussian basis set used[a].

Centre	Type	Exponent
C	s	0.043 70, 0.017 25
	p	0.021 06
	d	1.20, 0.35
O	s	0.0608, 0.024
	p	0.028
	d	1.40, 0.45
CM[b]	s	0.025, 0.005
	p	0.025, 0.005
	d	0.025

[a] In addition to the [10s6p]/(5s4p) set of Dunning (1971).
[b] Centre of mass.

Table 2. Calculated properties of target wavefunctions.

State	Dipole moment[a] (Debye)	$\langle R^2 \rangle$[c]	Vertical (IVO)[d]	Threshold (eV) (ROHF)[e]
X $^1\Sigma^+$	0.267[b]			—
B $^1\Sigma^+(3s\sigma)$	3.65	59.32	12.05	10.02
b $^3\Sigma^+(3s\sigma)$	2.71	38.72	11.15	9.93
E $^1\Pi^+(3p\pi)$	0.585	66.12	12.65	—

[a] Computed from the IVO wavefunctions.
[b] Experimental value +0.112 Debye.
[c] $\langle R^2 \rangle$ (au) for the relevant Rydberg orbital.
[d] Vertical excitation energy obtained using the IVO approximation for the excited state.
[e] Vertical excitation energy obtained with the RHF, relaxed-core approximation for the excited state.

d functions on each atom, together with a (2s2p2d) set of bond functions (see table 1). This basis gives a total of 38 σ, 32 π and 5 δ virtual orbitals in which to expand the scattering electron's wavefunction. All calculations were carried out in the fixed-nuclei approximation at the equilibrium geometry of the ground state ($R = 2.132$ au). This basis gives a ground-state SCF energy of $-112.782\,059$ au and dipole moment -0.105 au (experimental value $+0.044$ au). Some properties of the wavefunctions used in the cross section calculations are summarized in table 2. The calculated excitation energies differ from the measured values (see table 3) due to our use of uncorrelated SCF-like wavefunctions. We therefore report cross sections relative to the appropriate experimental threshold energies.

The IVO method neglects relaxation effects: the orbital into which excitation occurs is computed in the field of molecular orbitals taken from the ground-state SCF calculation (one of which is singly occupied). This 'frozen-core' approximation simplifies the evaluation of matrix elements between states and is required by our present computer programs, but in some cases it gives a poor representation of the excited state. For Rydberg orbitals, in particular, a relaxed-core description that uses the orbitals of the positive ion may be preferable and can provide useful insights. To assess the importance of relaxation, we have performed limited scattering calculations using the positive-ion orbitals for both the ground and the excited state. Results from these calculations will be compared below with results from calculations based on the IVO approximation.

Various channel-coupling schemes were considered to determine where calculations beyond a simple two-channel approximation could be useful. For the b $^3\Sigma^+$ and E $^1\Pi$ states, the two-channel approximation was adequate, but results for the B $^1\Sigma^+$ state indicate that cross sections for this transition are strongly affected by coupling to other channels,

Table 3. Electron configurations and properties of some electronic states of CO.

Electronic state	Electronic structure of CO: Valence orbitals KL[a]	1π	5σ	2π	6σ	Rydberg orbitals 3s	3pσ	3pπ	Energy of the $v=0$ vibrational level (eV)	Dipole moment (Debye)[e]	Equilibrium internuclear distance r_e (Å)[j]
X $^1\Sigma^+$	KL	4	2	—	—	—	—	—[b]	0	0.112 ± 0.005[f]	1.128
b $^3\Sigma^+$	KL	4	1	—	—	1	—	—[b]	10.399[d]	2.258[g]	1.113
B $^1\Sigma^+$	KL	4	1	—	—	1	—	—[b]	10.777[d]	1.60 ± 0.15[h]	1.119
j $^3\Sigma^+$	KL	4	1	—	—	—	1	—[c]	11.269[d]		1.144
C $^1\Sigma^+$	KL	4	1	—	—	—	1	—[b]	11.396[d]	$(-)4.50 \pm 0.07$[i]	1.122
c $^3\Pi$	KL	4	1	—	—	—	—	1[c]	11.414[d]		1.127
E $^1\Pi$	KL	4	1	—	—	—	—	1[b]	11.524[d]		1.115

[a] KL describes the doubly occupied core orbitals: $1\sigma^2 2\sigma^2 3\sigma^2 4\sigma^2$.
[b] Krupenie (1966).
[c] Chung and Lin (1974).
[d] Hammond *et al* (1985).
[e] A positive value indicates polarity C^+O^-.
[f] Kopelman and Klemperer (1962).
[g] Calculated value of Weatherford and Huo (1990).
[h] Fisher and Dalby (1976).
[i] Drabbels *et al* (1993).
[j] Huber and Herzberg (1979).

especially at energies above 20 eV. We therefore report cross sections for the B $^1\Sigma^+$state (frozen-core wavefunction) from a five-channel calculation in which the X $^1\Sigma^+$, b $^3\Sigma^+$, j $^3\Sigma^+$ and C $^1\Sigma^+$ states were coupled to the B $^1\Sigma^+$ state. All relaxed-core results reported were obtained in the two-channel approximation.

3. Resonances in the excitation functions of the Rydberg states

Sharp structures seen in the excitation functions of the Rydberg states of CO feature prominently in the integral cross sections shown in figure 1. These structures arise from core-excited shape and Feshbach resonances (negative-ion states). Such core-excited resonances can be built by adding an electron to a parent state, which for the transitions considered in this paper is one of the Rydberg states of the neutral molecule. Some relevant properties of the Rydberg states of CO of interest in these studies are summarized in table 3.

Feshbach and core-excited shape resonances are distinguished by the position of the negative ion state with respect to the associated parent state. The energy of a Feshbach resonance lies below that of its parent, preventing the decay of the resonance into the parent channel and leading to long lifetimes. Hence, Feshbach resonances characteristically appear as very narrow, sharply defined structures in multiple channels. A core-excited shape resonance, however, can decay into the parent state. The presence of this decay channel reduces the lifetime of core-excited shape resonances to 10^{-15}–10^{-14} s. Typically, core-excited shape resonances are much broader than Feshbach resonances and appear prominently only in the excitation function for the associated parent state. Whereas Feshbach resonances are usually associated with Rydberg parents, core-excited shape resonances can also be associated with valence parent states.

A helpful method for describing the binding mechanism of a core-excited Feshbach resonance has been given by Schulz (1973; see also Brunt *et al* 1978). The two outermost

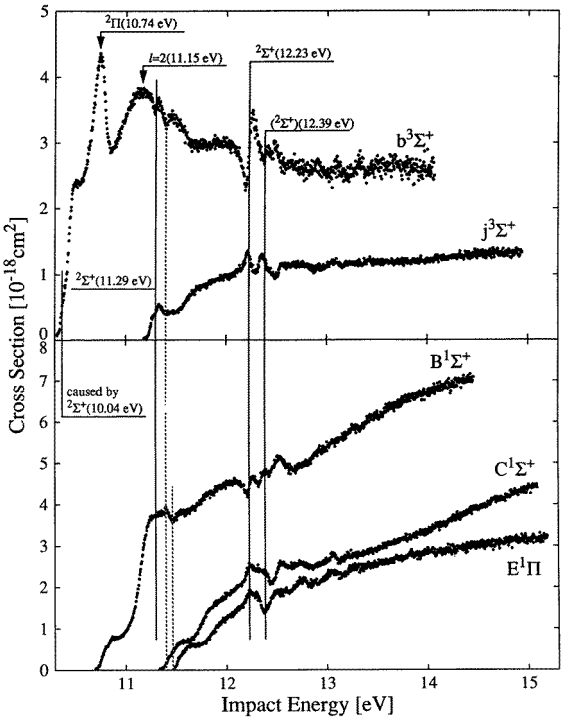

Figure 1. Energy dependence of the integral cross sections of the vibrationally elastic transitions from the X $^1\Sigma^+$ ($v = 0$) ground state into the b $^3\Sigma^+$, B $^1\Sigma^+$, j $^3\Sigma^+$, C $^1\Sigma^+$ and E $^1\Pi$ Rydberg states of CO. Note the threshold peak in the b $^3\Sigma^+$ state caused by the decay of the $^2\Sigma^+$ ($v = 0$) Feshbach resonance at 10.04 eV. Structures caused by core-excited shape resonances are indicated with arrows, those caused by Feshbach resonances with full lines, and those probably caused by the opening of electronic states with broken lines.

electrons, those in the Rydberg orbitals, couple together in the field of the singly charged positive ion, the so-called 'grandparent state', to form a resonance with well defined total spin and, for linear molecules, angular momentum about the molecular axis. The vibrational structure of the resonance is similar to that of the grandparent state, because the two coupled electrons are captured in non-bonding Rydberg orbitals (Sanche and Schulz 1972). In the case of CO^+, two vibrational levels are known for the X $^2\Sigma^+$ state, while a sequence of narrowly spaced levels has been observed for the A $^2\Pi$ state. These vibrational levels should be reflected in the energy positions of Feshbach resonances associated with these grandparent cation states.

Feshbach resonances in the electronic excitation of CO have been observed in metastable excitation functions (Newman *et al* 1983, Brunt *et al* 1978) and in total electron-impact cross sections (see, e.g. Sanche and Schulz 1972, Polley and Bailey 1988). The modified Rydberg formula developed by Brunt *et al* (1978, and references therein) shows the orbital energies of the 3sσ, 3pσ and 3pπ electrons to be 3.52, 2.70 and 2.57 eV, respectively. Using these energies, the electronic configurations of several of the Feshbach resonances detected in the present experiments can be ascertained. These resonances are indicated in figure 1 by vertical lines, while the arrows indicate core-excited shape resonances. The respective properties of these resonances are given in table 4.

The $^2\Sigma^+$ (10.04 eV) Feshbach resonance

Just at the threshold of the b $^3\Sigma^+$ state, we observed a small but marked peak (figure 2) with a FWHM of the order of the experimental energy resolution. This peak is found to be isotropic—the angular behaviour expected from an sσ partial wave. Mazeau *et al* (1972) observed a similar angular distribution for the threshold peak, supporting the idea that the b $^3\Sigma^+$ state is excited at threshold via the $^2\Sigma^+$ ($v = 0$) Feshbach resonance at 10.044 eV.

Table 4. Energy positions and properties of some resonance states of CO.

Symmetry	Energy position (eV)	FWHM (ev)	Electron configuration	Resonance classification	Parent states
$^2\Pi$[a]	1.8	0.7–1.0	$kl\ 1\pi^4 5\sigma^2 2\pi^1$	shape resonance	X $^1\Sigma^+$
Π[b]	6.01 ± 0.02	0.08 ± 0.025	$kl\ 1\pi^4 5\sigma^2 2\pi^2$	dipole bound state	a $^3\Pi$
$^2\Pi$[c]	9.0 ± 0.1	1.2 ± 0.3	$kl\ 1\pi^3 5\sigma^2 2\pi^2$	core-excited shape resonance	a′ $^3\Sigma^+$
$^2\Delta$[d]	9.2		$kl\ 1\pi^4 5\sigma^1 2\pi^2$	core-excited shape resonance	a $^3\Pi$
$^2\Sigma^+$[d]	10.5		$kl\ 1\pi^4 5\sigma^1 2\pi^2$	core-excited shape resonance	a $^3\Pi$
$^2\Sigma^+$[e]	10.044 ± 0.01	0.045 ± 0.01	$kl\ 1\pi^4 5\sigma^2 3s\sigma^2$	Feshbach resonance	b $^3\Sigma^+$
$^2\Pi$[f]	10.74 ± 0.02	0.3 ± 0.15	$kl\ 1\pi^4 5\sigma^1 3s\sigma^1 3p\pi^1$	core-excited shape resonance	b $^3\Sigma+$
$(l = 2)$	11.15 ± 0.1	> 1.0		(core-excited shape resotiance)	(b $^3\Sigma^+$)
$^2\Sigma^+$[f]	11.29 ± 0.02		$kl\ 1\pi^4 5\sigma^1 3p\sigma^2$	Feshbach resdnance	
$^2\Sigma^+$[f]	12.23 ± 0.02		$kl\ 1\pi^4 5\sigma^1 4s\sigma^2$	Feshbach resonance	f $^3\Sigma+$, F $^1\Sigma^+$
($^2\Sigma^+$)[g]	12.39 ± 0.03		($kl\ 1\pi^4 5\sigma^1 4p\sigma^2$)[g]	(Feshbach) resonance[g]	
$^2\Sigma^+$[h]	16.2			(core-excited) shape resonance	

[a] An overview of measured and calculated results is given by Jain and Norcross (1992).
[b] Zobel *et al* (1994) and references therein.
[c] Observed at 1.3 ± 0.1 eV above the a′ $^3\Sigma^+$ ($v = 6$) state at 7.714 eV (see paper I).
[d] Values of the maxima in the resonant contributions to the calculated a $^3\Pi$ cross section of Morgan and Tennyson (1993).
[e] Comer and Read (1971).
[f] Electron configurations and classification taken from Newman *et al* (1983). See the text for further details.
[g] Newly detected resonance with suggested electron configuration and symmetry.
[h] Weatherford and Huo (1990).

Table 5. Measured differential cross sections (10^{-18} cm^2 sr^{-1}) for the X $^1\Sigma^+$ ($v = 0$) $\rightarrow$ b $^3\Sigma^+$ ($v = 0$) excitation. The excitation threshold is 10.40 eV.

	ϑ												
E_d	20°	30°	40°	50°	60°	70°	80°	90°	100°	110°	120°	130°	140°
0.34	0.95	0.97	0.66	0.47	0.35	0.37	0.21	0.18	0.14	0.11	0.20	0.40	0.47
0.8	0.30	0.31	0.28	0.29	0.31	0.34	0.36	0.39	0.34	0.28	0.27	0.23	0.19
1.8	0.28	0.28	0.27	0.26	0.24	0.21	0.20	0.17	0.17	0.16	0.16	0.16	0.15
2.74	—	—	—	—	0.32	0.27	0.21	0.19	0.14	0.12	0.13	0.12	0.13
3.7	0.39	0.39	0.34	0.32	0.29	0.25	0.19	0.16	0.13	0.12	0.13	0.15	0.19

The electronic configuration of this resonance has been taken to be $KL1\pi^4 5\sigma 3s\sigma^2$, with the b $^3\Sigma^+$ state (electronic configuration $KL1\pi^4 5\sigma 3s\sigma$) as the parent state (Sanche and Schulz 1972; see also Newman *et al* 1983, Comer and Read 1971, Swanson *et al* 1975, Mazeau *et al* 1972).

The $^2\Pi$ (10.76 eV) core-excited shape resonance

A strong peak with a FWHM of 0.3 ± 0.15 eV is observed in the cross section of the b $^3\Sigma^+$ state at 10.74 ± 0.02 eV. As can be seen in figure 3(*a*), the angular dependence of this peak is consistent with a pπ partial wave. Mazeau *et al* (1972), Newman *et al* (1983) and Brunt *et al* (1978) interpreted this angular behaviour in terms of a core-excited shape resonance of $^2\Pi$ symmetry (electronic configuration $KL1\pi^4 5\sigma 3s\sigma 3p\pi$) with the X $^2\Sigma^+$ ion as the grandparent state.

The $l = 2$ (11.15 eV) resonance

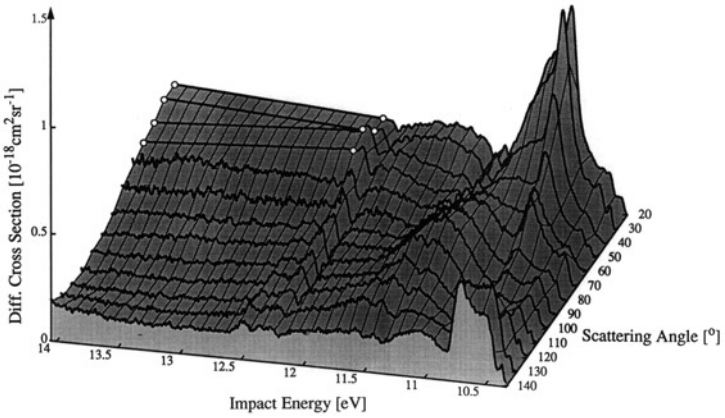

Figure 2. Energy dependence of the absolute differential cross section for electronic excitation of the b $^3\Sigma^+$ ($v = 0$) state of CO.

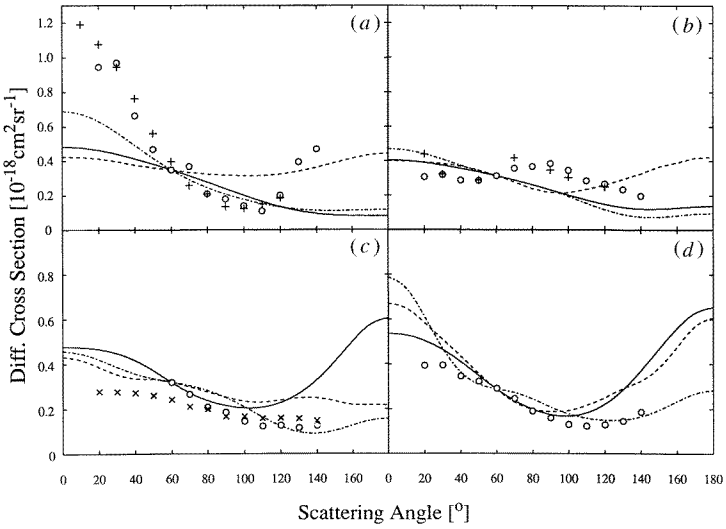

Figure 3. Differential cross section for the X $^1\Sigma^+$ ($v = 0$) $\rightarrow$ b $^3\Sigma^+$ ($v = 0$) excitation. (*a*) ——, present calculations using the IVO approximation; — · —, present results using a relaxed core; – – –, calculation of Weatherford and Huo (1990) at a detection energy of 0.19 eV; ○, present measured values at the maximum of the $^2\Pi$ (10.74 eV) resonance (detection energy 0.34 eV); +, experimental results of Mazeau *et al* (1972) normalized to our measured value at 80° (detection energy 0.3 eV). (*b*) ——, present IVO calculations; — · —, present results using a relaxed core; – – –, calculation of Weatherford and Huo (1990) at 1.04 eV above threshold; ○, present measurements at 11.2 eV (detection energy 0.8 eV); +, angular behaviour at 11.2 eV measured by Mazeau *et al* (1972) and normalized to our measured value at 50°. (*c*) ——, present IVO calculations; — · —, results with a relaxed-core wavefunction; – – –, calculation of Weatherford and Huo (1990) at a detection energy of 2.74 eV; ○, present measured results at a detection energy of 2.74 eV; ×, present results at a detection energy of 1.8 eV. (*d*) ——, present IVO calculations; — · —, present results using a relaxed core; – – –, calculation of Weatherford and Huo (1990) at 5.34 eV above threshold; ○, present measurements at a detection energy of 3.7 eV.

A second but much broader hump overlapping with the $^2\Pi$ resonance at 10.76 eV is observed at 11.15 ± 0.1 eV in the cross section of the b $^3\Sigma^+$ state. The FWHM of this hump cannot be determined from our measurements due to other overlapping excitation features at this impact energy. Nevertheless, the FWHM seems to be greater than 1 eV. Mazeau *et al* (1972; see also Reinhardt *et al* 1972) observed this structure in their excitation functions and estimated the FWHM to be 0.7 eV. This large width is indicative of a core-excited shape resonance. The angular behaviour of this resonant feature, shown in figure 3(*b*) along with the results of Mazeau *et al* (1972), is probably due to a d-wave ($l = 2$), but the precise symmetry of the resonance is uncertain.

The $^2\Sigma^+$ (11.29 eV) Feshbach resonance

At 11.29 ± 0.02 eV the Fano–Beutler profile of a Feshbach resonance is evident in the cross sections of the b $^3\Sigma^+$ state in figures 1 and 2. On the basis of the modified Rydberg formula, Newman *et al* (1983) attributed this resonance to a $KL1\pi^4 5\sigma 3p\sigma^2$ ($^2\Sigma^+$) electronic configuration. Besides the b $^3\Sigma^+$ channel, this resonant structure only appears in the cross section of the j $^3\Sigma^+$ state. There the maximum of the feature is shifted to higher energy due to interference with the non-resonant scattering background.

The $^2\Sigma^+$ (12.23 eV) Feshbach resonance

A strong resonant feature at 12.23 ± 0.02 eV appears in the measured cross sections of all the states. Newman *et al* (1983) suggested that the electronic configuration of this resonance is $KL1\pi^4 5\sigma 4s\sigma^2$ ($^2\Sigma^+$). Mazeau *et al* (1975) have suggested that the parent states are the F $^1\Sigma^+$ and f $^3\Sigma^+$ Rydberg states.

A new resonance at 12.39 eV

A previously unreported structure was found in all measured cross sections at 12.39 ± 0.03 eV. It is best seen as a strong peak in the cross section of the j $^3\Sigma^+$ state in figure 1. The sharp Fano–Beutler profile, observable in the differential cross section of this state, indicates that this structure probably arises from a Feshbach resonance. Due to the non-resonant background, the maximum of the feature in the integral cross section of the j $^3\Sigma^+$ state is located below the resonance position. A possible electronic configuration for this resonant state is $KL1\pi^4 5\sigma 4p\sigma^2$. This would be in agreement with the sequence of the orbital configurations and energy positions of the resonances suggested by Newman *et al* (1983). The symmetry of this Feshbach resonance would therefore be $^2\Sigma^+$.

The structures appearing in the cross sections of the b $^3\Sigma^+$ and B $^1\Sigma^+$ states, shown by the broken lines in figure 1, probably result from the opening of the electronic states C $^1\Sigma^+$, c $^3\Pi$ and E $^1\Pi$ (see also Newman *et al* 1983).

4. Cross sections

The b $^3\Sigma^+$ state

The measured excitation function of the b $^3\Sigma^+$ state, the lowest Rydberg state of CO, reveals complex resonant structures within the first 2 eV above threshold (figures 1 and 2). The structures above the threshold peak seen here are in agreement with those found in the relative cross sections at 40°, 70° and 90° by Mazeau *et al* (1972), who attributed this threshold peak to the overlap of the tail of the resonance at 10.04 eV with the b $^3\Sigma^+$

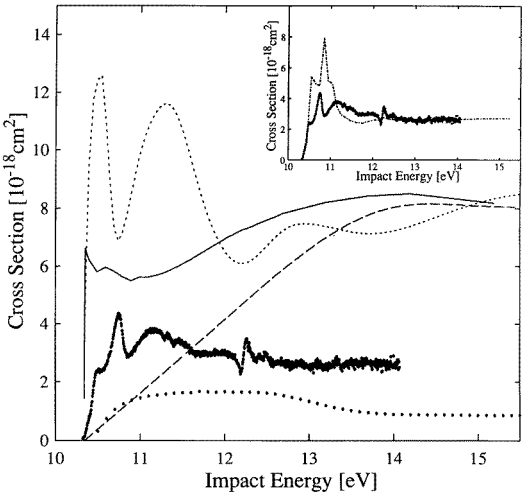

Figure 4. Energy dependence of the integral cross section for the X $^1\Sigma^+ \rightarrow$ b $^3\Sigma^+$ excitation. The calculated curves are shifted to the experimental threshold. (*a*) ●, present experimental results; ——, present calculations using the IVO approximation; – – –, calculations of Weatherford and Huo (1990); — · —, calculations of Chung and Lin (1974); — — —, experimental results of Land (1978); · · · · · ·, experimental results of Skubenich (1967). The inset compares results of calculations using the relaxed-core approximation with present measurements (see the text). The theoretical values have been normalized to experiment at 14 eV.

threshold. At energies slightly above the threshold peak, we found a steep onset of the differential cross section similar to the rapid rise at the threshold of the a $^3\Pi$ valence state of CO. In the latter case, the low-lying (1.8 eV) $^2\Pi$ shape resonance is responsible for this steep onset (paper I). There are no resonances known to lie below the threshold of the b $^3\Sigma^+$ state that can decay into this state.

Our measured and calculated integral cross sections are compared with the calculated cross sections of Chung and Lin (1974) and of Weatherford and Huo (1990) and with the measurements of Skubenich (1967) and Land (1978) in figure 4. The measured integral cross section at threshold seems to consist of an overlap of the low-energy wings of the $^2\Pi$ (10.74 eV) core-excited shape resonance with the $l = 2$ (11.15 eV) resonance. The Ochkur–Rudge calculations of Chung and Lin (1974) would not be sensitive to effects arising from shape or Feshbach resonances. Similarly, the cross sections of Land were derived from fitting to electron transport properties obtained from swarm experiments, which are insensitive to narrow features.

In principle, the cross sections of Weatherford and Huo and the present calculated results should be very similar. However, in the present calculations we used an improved quadrature to evaluate a class of matrix elements occurring in equation (1). Our experience has shown that cross sections near thresholds and in the presence of resonances are sensitive to these terms. Indeed, Weatherford and Huo observe features near threshold that do not appear in the present calculations, whereas the two calculations converge at higher energies (figure 4). Except for the resonance-like features observed by Weatherford and Huo, the two SMC calculations show similar behaviour. In particular, the $^2\Sigma$ symmetry dominates the cross sections at all energies. Also, a very rapid rise of the cross section near threshold (< 0.1 eV) is seen in both calculations. Although the present results are in somewhat better agreement with experiment at low energies, the SMC method still yields cross sections approximately twice as large as the measured values near threshold. As noted by Weatherford and Huo (1990), the SMC cross sections are also about two to three times larger than the measured cross section of Trajmar *et al* (1973) at 20 eV.

Comparison of our measured values with the differential cross sections calculated using the frozen-core wavefunction for the excited state reveals qualitative differences (figures 3(*a*)–(*d*)). To aid in comparing shapes, all calculated DCSs have been normalized to the measured values at 60°. The measured DCS near the $^2\Pi$ (10.76 eV) resonance exhibits the

expected minimum near 90°. The calculated DCS of Weatherford and Huo shows dominant contribution from an incident s-wave and an exit pσ-wave. Our present calculated DCS is more forward peaked. Limited multichannel calculations did not show any enhancement in the p-wave character that is evident in the measured DCS. Likewise, the d-wave character expected near the $l = 2$ (11.15 eV) resonance is seen in the measured but not in the calculated DCS.

Following Weatherford and Huo, we also performed a calculation in which the threshold for excitation of the b $^3\Sigma^+$ state was set at 0.4 eV above the IVO energy of the $KL1\pi^4 5\sigma 3s\sigma^2$ configuration responsible for the $^2\Sigma^+$ Feshbach resonance. We observed little qualitative change in the cross sections, a result also reported by Huo and Weatherford.

To assess the influence of core relaxation on the behaviour of these cross sections, we also carried out calculations with relaxed-core orbitals obtained from a restricted open-shell Hartree–Fock (ROHF) calculation on the b $^3\Sigma^+$ state, instead of the IVO orbitals, to describe the ground and excited states of the target. Although the integral cross sections are much larger than those obtained using the frozen-core IVO approximation, *qualitative* agreement with experiment is much improved. The inset in figure 4 compares the integral cross sections obtained using the relaxed core orbitals, scaled by a factor of 0.2, with the measured cross sections. As with the IVO calculations, there is a rapid rise in the cross section near threshold, again in the $^2\Sigma$ symmetry. However, a resonance now appears in the $^2\Pi$ symmetry that was not observed using the IVO orbitals. At higher energies, the d-wave behaviour of the measured DCSs is reflected to some degree in the calculated cross sections, as shown by the chain curves in figures 3(*c*) and (*d*). Such d-wave character was not observed in any of the IVO cross sections up to 20 eV. It thus appears that relaxation of the core of the b $^3\Sigma^+$ state affects the excitation dynamics near threshold.

The B $^1\Sigma^+$ state

The potential curve of the B $^1\Sigma^+$ state of CO is crossed at larger internuclear distances by that of the D′ $^1\Sigma^+$ state (Cooper and Kirby 1987, Wolk and Rich 1983, Coughran *et al* 1973), and therefore only four vibrational states are known for the B $^1\Sigma^+$ state (Kirby and Cooper 1989, Baker *et al* 1995). Furthermore, the $v = 2$ and $v = 3$ levels are only observed in the absorption spectrum (Eidelsberg *et al* 1987, Baker *et al* 1995) due to predissociation (Viala *et al* 1988, Cooper and Langhoff 1981).

The energy dependence of the measured differential cross section for the X $^1\Sigma^+$ ($v = 0$) $\rightarrow$ B $^1\Sigma^+$ ($v = 0$) transition is given in figure 5. These differential cross sections are also shown in table 6. This cross section shows the strong scattering at small angles characteristic of dipole-allowed excitations.

As in the case of the b $^3\Sigma^+$ state, we found it useful to obtain cross sections for the B $^1\Sigma^+$ state both in the IVO (frozen-core) and in the relaxed-core ROHF approximations. The ROHF calculations were carried out at the two-state level. In figure 6, the IVO (full curve) and ROHF (chain curve) cross sections are compared with the measured values. Both of the calculated cross sections are considerably larger than experiment. The IVO calculations show a prominent $^2\Pi$ peak near threshold, with a second, broader maximum in the same symmetry at about 12.6 eV. The structure seen in the frozen-core IVO cross section near 11.4 eV is a consequence of the opening of the j $^3\Sigma^+$ state. The ROHF results do not show the $^2\Pi$ peak near threshold. This may be a reflection of the reduction in the permanent dipole moment of the B $^1\Sigma^+$ state, from 3.60 D (IVO) to 2.33 D (ROHF). The measured integral cross sections exhibit the non-resonant behaviour expected from the Wigner threshold law within the first 200 meV of threshold. The strong threshold peak found by Mazeau *et al* (1972) at 60° and by Swanson *et al* (1975) at 45° was not observed. The latter group

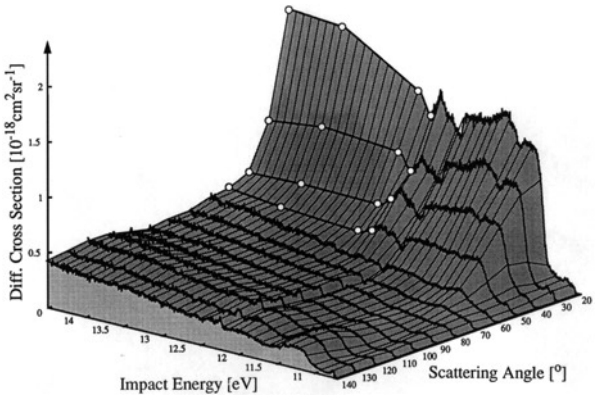

Figure 5. Energy dependence of the absolute differential cross section for electronic excitation of the B $^1\Sigma^+$ ($v = 0$) state of CO.

Table 6. Measured differential cross sections (10^{-18} cm^2 sr^{-1}) for the X $^1\Sigma^+$ ($v = 0$) $\rightarrow$ B $^1\Sigma^+$ ($v = 0$) excitation. The excitation threshold is 10.78 eV.

	ϑ												
E_d	20°	30°	40°	50°	60°	70°	80°	90°	100°	110°	120°	130°	140°
0.1	0.059	0.064	0.066	0.064	0.068	0.064	0.061	0.053	0.042	0.035	0.033	0.047	0.037
0.3	0.28	0.26	0.22	0.18	0.14	0.10	0.07	0.05	0.04	0.05	0.06	0.09	0.11
0.8	1.21	0.94	0.62	0.40	0.24	0.15	0.11	0.12	0.12	0.13	0.14	0.17	0.15
1.3	1.36	1.03	0.66	0.42	0.28	0.22	0.20	0.21	0.26	0.24	0.24	0.24	0.21
2.0	1.46	0.98	0.58	0.39	0.30	0.28	0.26	0.28	0.29	0.21	0.31	0.20	0.27
3.0	1.88	1.04	0.59	0.44	0.40	0.37	0.25	0.26	0.39	0.42	0.43	0.41	0.37
3.7	1.92	0.98	0.57	0.49	0.44	0.41	0.29	0.38	0.43	0.46	0.47	0.44	0.42

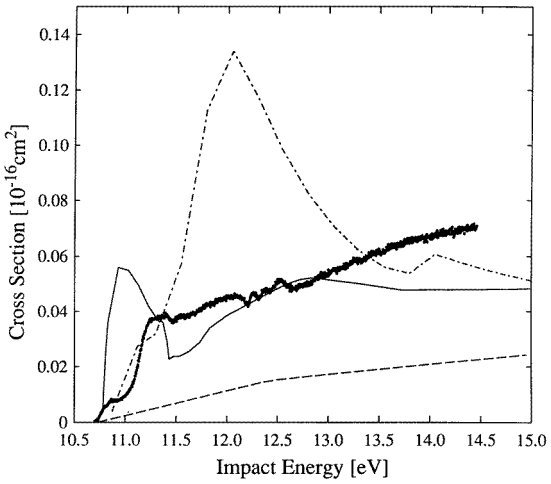

Figure 6. Energy dependence of the integral cross section for the X $^1\Sigma^+$ ($v = 0$) $\rightarrow$ B $^1\Sigma^+$ ($v = 0$) excitation: ●, present measurements; ——, present IVO (frozen-core) calculations; — · —, present relaxed-core results; – – –, Skubenich (1967).

assumed that this peak is caused by an enhanced sensitivity of the detector to electrons with very low energies; in the measurements of Allan (1989) at $0^\circ + 180^\circ$, a steep onset without a threshold peak was found.

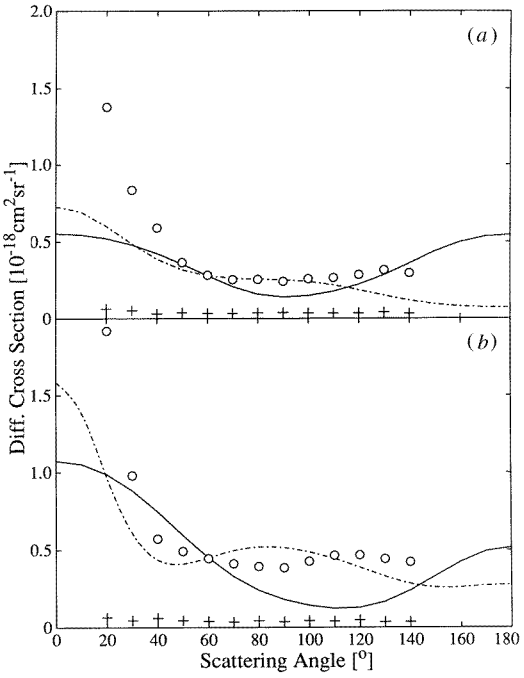

Figure 7. Angular behaviour of the X $^1\Sigma^+ \rightarrow$ B $^1\Sigma^+$ electronic excitation. ——, present calculations using the IVO approximation; — · —, calculations using the relaxed-core model; ○, present measurements for $v = 0 \rightarrow 0$; +, present measurements for $v = 0 \rightarrow 1$ at detection energies of (*a*) 1.8 eV, (*b*) 3.7 eV.

Comparison of the measured differential cross sections with the cross sections calculated using the IVO and relaxed-core models of the target indicates that, as with the b $^3\Sigma^+$ state, the latter are in better qualitative agreement with experiment. At 1.8 eV above threshold (figure 7(*a*)), the IVO cross sections (full curve) reflect the dominant $^2\Pi$ contribution, while the relaxed-core results (chain curve; normalized to experiment at 60°) more accurately reflect the non-resonant appearance of the measured cross sections. At 3.7 eV (figure 7(*b*)), the shape of the relaxed-core cross section again more closely resembles that of the measured cross section.

From the energy-loss spectra we could also obtain the absolute differential cross sections for the X $^1\Sigma^+$ ($v = 0$) $\rightarrow$ B $^1\Sigma^+$ ($v = 1$) excitation at detection energies of 1.8 eV and 3.7 eV (figures 7(*a*) and (*b*)). Like Klump and Lassettre (1974), we find an unusual ratio of the vibrationally elastic to the vibrationally inelastic scattering. For further discussion of this non-Franck–Condon behaviour, see Skerbele and Lassettre (1974), James *et al* (1992), and Lassettre and Skerbele (1974).

The j $^3\Sigma^+$ state

Excitation of the spin-forbidden X $^1\Sigma^+$ ($v = 0$) $\rightarrow$ j $^3\Sigma^+$ ($v = 0$) transition has an extremely low intensity, resulting in a rather poor signal-to-noise ratio. Nonetheless, a small resonance structure is detected just above the threshold, which we attribute to the $^2\Sigma^+$ Feshbach resonance at 11.29 eV (figure 1). This Feshbach resonance close to the threshold (11.264 eV) of the j $^3\Sigma^+$ state is probably the reason for the uncertainties in the determination of the excitation energy of this state (Swanson *et al* 1975, Middleton *et al* 1993).

The smooth rise in the integral cross section (figure 1), starting at about 11.6 eV impact energy, cannot readily be attributed to a resonant excitation process, since the angular

distribution is not dominated by a single partial wave. This behaviour was observed over the entire energy range.

Ochkur–Born calculations of Chung and Lin (1974) show a cross section about three times larger than our measured values.

The C $^1\Sigma^+$ state

Although the C $^1\Sigma^+$ ($v = 0$) state at 11.397 eV cannot be separated from the c $^3\Pi$ ($v = 0$) state at 11.414 eV, we attempted to study the excitation of the C $^1\Sigma^+$ state by choosing an energy at the half height of the energy-loss peak on the low-energy side of the two overlapping states.

The C $^1\Sigma^+$ state has a large enough dipole moment, 4.50 D (Fisher and Dalby 1976), to bind an electron. However, no structures similar to those at the excitation energy (6.01 eV) of the a $^3\Pi$ ($v = 0$) state in the cross section for vibrational excitation ($v = 0 \rightarrow 1$) of the X $^1\Sigma^+$ state of CO (Zobel *et al* 1994), which are due to a dipole bound state, are found at the energy position of the C $^1\Sigma^+$ ($v = 0$) state.

The differential cross sections shown in figures 8 and 9 and in table 7 are normalized at 3.7 eV above threshold to the absolute values of the energy-loss peaks. Therefore the entire contribution of the c $^3\Pi$ state at the normalization points is included, undoubtedly leading to an overestimation of the true cross sections. Nevertheless, the measured differential cross sections (figure 8) show behaviour typical of a $^1\Sigma^+ \rightarrow {}^1\Sigma^+$ transition, obeying the $\sigma \propto E^{l+1/2}$ ($l = 0$) behaviour predicted from the Wigner threshold law within the first 200 meV above threshold (see also the integral cross section in figure 1). At 0.2 eV above threshold, the angular dependence is found to be essentially isotropic (figure 9), while at higher energies, the differential cross sections show the pronounced forward peaking expected for a dipole-allowed transition.

Table 7. Measured differential cross sections (10^{-18} cm^2 sr^{-1}) for the X $^1\Sigma^+$ ($v = 0$) $\rightarrow$ C $^1\Sigma^+$ ($v = 0$) excitation. The excitation threshold is 11.40 eV.

	ϑ												
E_d	20°	30°	40°	50°	60°	70°	80°	90°	100°	110°	120°	130°	140°
0.2	0.054	0.045	0.041	0.033	0.041	0.052	0.052	0.049	0.053	0.056	0.068	0.085	0.071
1.8	0.47	0.32	0.28	0.23	0.24	0.23	0.23	0.21	0.21	0.19	0.18	0.19	0.15
3.7	1.15	0.64	0.41	0.37	038	0.35	0.35	0.29	0.28	0.22	0.21	0.17	0.17

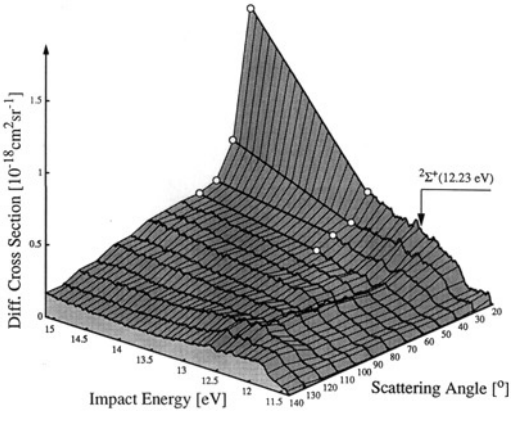

Figure 8. Energy dependence of the absolute differential cross section for electronic excitation of the C $^1\Sigma^+$ ($v = 0$) state of CO.

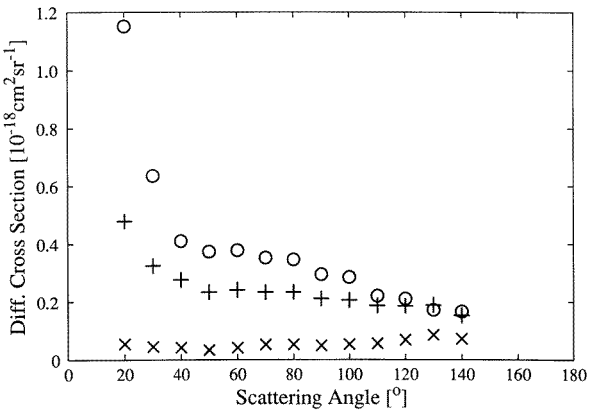

Figure 9. Angular dependence of the differential cross section for the X $^1\Sigma^+$ ($v = 0$) $\rightarrow$ C $^1\Sigma^+$ ($v = 0$) transition at impact energies of 11.6 eV (×), 13.2 eV (+) and 15.1 eV (○).

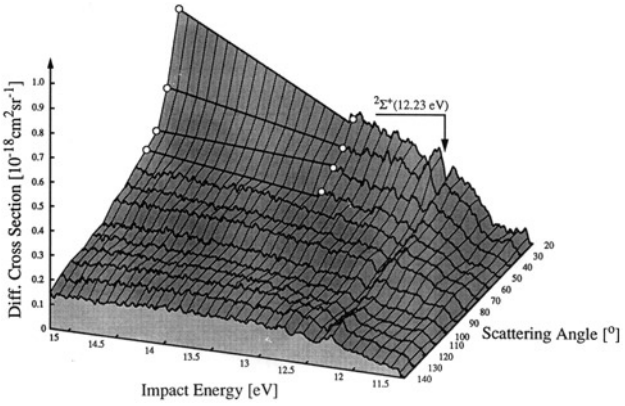

Figure 10. Energy dependence of the absolute differential cross section for excitation of the E $^1\Pi$ ($v = 0$) state of CO.

Table 8. Measured differential cross sections (10^{-18} cm^2 sr^{-1}) for the X $^1\Sigma^+$ ($v = 0$) $\rightarrow$ E $^1\Pi$ ($v = 0$) excitation. The excitation threshold is 11.52 eV.

	ϑ												
E_d	20°	30°	40°	50°	60°	70°	80°	90°	100°	110°	120°	130°	140°
0.25	0.052	0.043	0.048	0.038	0.051	0.064	0.072	0.056	0.044	0.045	0.051	0.059	0.052
1.8	0.41	0.21	0.29	0.24	0.22	0.20	0.19	0.15	0.16	0.15	0.16	0.17	0.16
3.7	0.76	0.48	0.35	0.22	0.29	0.25	0.23	0.19	0.20	0.18	0.18	0.16	0.14

The E $^1\Pi$ state

Figure 10 and table 8 show our measured differential cross sections for excitation of the X $^1\Sigma^+$ ($v = 0$) $\rightarrow$ E $^1\Pi$ ($v = 0$) transition. In figure 11 the integral cross section derived from these measured DCS is compared with the results of our IVO (full curve) and relaxed-core (chain curve) calculations. The relaxed-core results are normalized to the measured value of the DCS at 60° at an energy of 15.22 eV. The resonance feature seen in the IVO cross sections near 12.4 eV arises from the $^2\Sigma^+$ symmetry component of the total (electron plus molecule) scattering wavefunction. Analysis of the wavefunction around this energy shows the dominant configuration to be $KL1\pi^4 5\sigma 3p\pi^2$ and not $KL1\pi^4 5\sigma 4s\sigma^2$. The integral cross section obtained from the IVO calculation agrees quite well with experiment.

The measured cross sections show only small deviations from the $\sigma \propto E^{1/2}$ behaviour

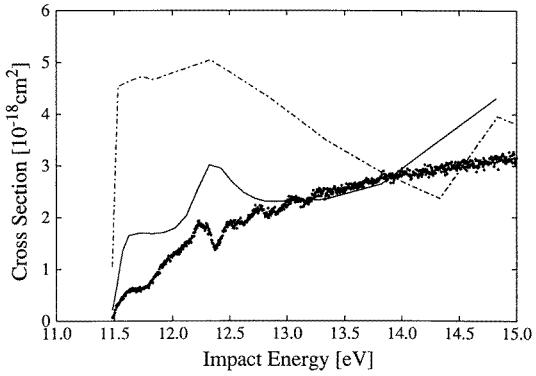

Figure 11. Energy dependence of the integral cross section for excitation of the E $^1\Pi$ ($v = 0$) state of CO. — — —, present IVO (frozen-core) calculations; — · —, present relaxed-core results; ●, present measurements.

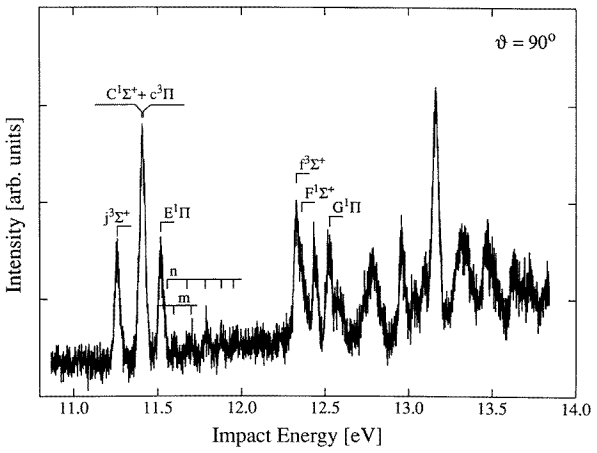

Figure 12. Constant residual energy spectrum of CO close (70 meV) to the excitation threshold at 90°. Values for the energy positions of the vibrational levels of the excited states are taken from Hammond *et al* (1985) and Wallbank *et al* (1983).

expected from Wigner's law. A possible explanation for these differences would include the effects of the dipole moment and of the polarizability in connection with the generalized threshold laws developed by O'Malley (1965) (see also the correction in Farley (1989)). However, the state does not possess a large dipole moment (−0.203 au in the present calculations). On the other hand, it is possible that a second state, not resolved experimentally, is responsible for the behaviour of the cross section at threshold. Simmons and Tilford (1974; see also Amiot *et al* 1986) observed an unexpected enhancement in the absorption spectrum, which was attributed to perturbation of the R(30) and P(32) rotational levels of the vibrational ground state of the E $^1\Pi$ state by a nearby state. Klopotek and Vidal (1985) (see also Wolk and Rich, 1983) showed in a two-step photoexcitation measurement that the perturbing state must be of Σ^+ symmetry, most probably a singlet. This state may contribute to the cross section at the threshold of the E $^1\Pi$ state. The only known nearby electronic states are the m and n states described by Hammond *et al* (1985) and Wallbank *et al* (1983). Figure 12 shows a constant residual energy spectrum taken at a detection energy of 70 meV, in which the lowest vibrational levels of the m and n states are identified. It can be seen that only the $v = 0$ level of the m state overlaps with the energy-loss peak of the E $^1\Pi$ state. Assuming the intensity of this vibrational level to be similar to that of the higher vibrational levels, it seems possible that the small deviations of the cross section of the E $^1\Pi$ state at threshold to the expected $\sigma \propto E^{1/2}$ behaviour is caused by the influence of the m ($v = 0$) state.

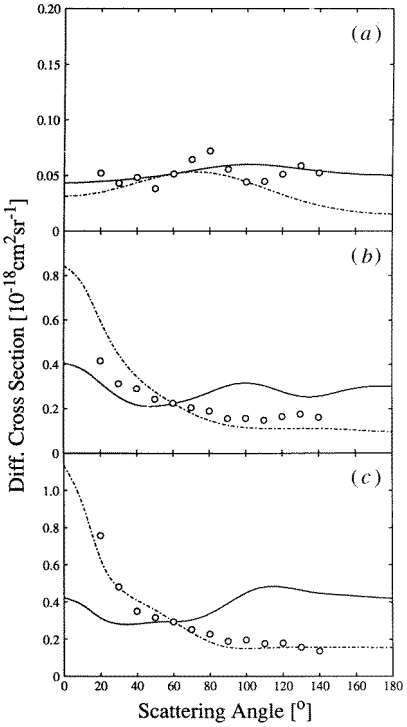

Figure 13. Angular dependence of the differential cross section of the X $^1\Sigma^+ \rightarrow$ E $^1\Pi$ transition: — — —, present calculations with frozen-core IVO wavefunctions; — · —, present results with relaxed-core wavefunctions; ○, present measurements for $v = 0 \rightarrow 0$ at impact energies of (*a*) 11.77 eV, (*b*) 13.32 eV and (*c*) 15.22 eV.

The measured and calculated differential cross sections are compared in figures 13(*a*)–(*c*) at energies of 11.72, 13.32 and 15.22 eV, respectively. Near threshold, the cross sections obtained from both the IVO (full curve) and relaxed-core (chain curve) calculations are dominated by the s-wave contribution. At 13.32 and 15.22 eV, the relaxed-core cross sections are in better agreement with the measured values. In contrast to the frozen-core IVO results, the relaxed-core differential cross sections exhibit the forward peaking observed experimentally. As with the other Rydberg states studied in this paper, it appears necessary to account for core-relaxation effects in calculating excitation cross sections.

5. Conclusions

We have reported absolute measurements of the differential cross sections for near-threshold electron-impact excitation of several Rydberg states of CO. Resonance features observed in the cross sections correlate well with earlier measurements, with the exception of a previously unobserved Feshbach resonance at 12.39 eV. This feature is tentatively assigned to the electron configuration $KL1\pi^4 5\sigma 4p\sigma^2$.

Differential and integral cross sections calculated using the SMC method have been compared with the measured values for the b $^3\Sigma^+$, B $^1\Sigma^+$ and E $^1\Pi$ states. The agreement is only fair, at best. This is not surprising given the restrictions imposed on the calculations, namely, a single-configuration description of the target, common orbitals for the ground and excited states, and the inclusion of a small number of open channels and no closed channels. Our goal in undertaking these calculations was to obtain a qualitative description of the the excitation cross sections for these Rydberg states. To obtain even such a qualitative description, however, the core electrons must be allowed to relax toward a CO^+ structure.

In contrast, SMC calculations for the valence states of CO gave results in generally good agreement with available experimental data, even with the frozen-core approximation (Sun *et al* 1992, paper I).

Acknowledgments

Work at the California Institute of Technology was supported by a grant from the Air Force Office of Scientific Research. Calculations reported here were carried out using facilities of the JPL/Caltech Supercomputing Project, the US Air Force, and the Concurrent Supercomputing Consortium, which is supported in part by the National Science Foundation. The authors gratefully acknowledge the financial support of the Deutsche Forschungsgemeinschaft for the work at the Universität Kaiserslautern.

References

Allan M 1989 *J. Electron Spectrosc. Relat. Phenom.* **48** 219
Amiot C, Roncin J-Y and Verges J 1986 *J. Phys. B: At. Mol. Phys.* **19** L19
Baker J, Tchang-Brillet W-Ü L and Julienne P S 1995 *J. Chem. Phys.* **102** 3956
Brunt J N H, King G C and Read F H 1978 *J. Phys. B: At. Mol. Phys.* **11** 173
Chung S and Lin C L 1974 *Phys. Rev.* A **9** 1954
Comer J and Read F H 1971 *J. Phys. B: At. Mol. Phys.* **4** 1678
Cooper D and Kirby K 1987 *J. Chem. Phys.* **87** 424
Cooper D M and Langhoff S R 1981 *J. Chem. Phys.* **74** 1200
Coughran W, Rose J, Shibuya T-I and McKoy V 1973 *J. Chem. Phys.* **58** 2699
Drabbels M, Meerst W L and ter Meulen J J 1993 *J. Chem. Phys.* **99** 2352
Dunning F B 1971 *J. Chem. Phys.* **55** 716
Eidelsberg M, Roncin J-Y, Le Floch A, Launay F, Letzelter C and Rostas J 1987 *J. Mol. Spectrosc.* **121** 309
Farley J W 1989 *Phys. Rev.* A **40** 6286
Fisher N J and Dalby F W 1976 *Can. J. Phys.* **54** 258
Hammond P, King G C, Jureta J and Read F 1985 *J. Phys. B: At. Mol. Phys.* **18** 2057
Hipes P, Winstead C, Lima M and McKoy V 1990 *Proc. 5th Distributed Memory Computing Conf.* ed D W Walker and Q F Stout (Los Alamitos: IEEE Computer Society) p 498
Hunt W J and Goddard W A 1969 *Chem. Phys. Lett.* **3** 414
Jain A and Norcross D W 1992 *Phys. Rev.* A **45** 1644
James G K, Ajello J M, Kanik I, Franklin B and Shemansky D E 1992 *J. Phys. B: At. Mol. Opt. Phys.* **25** 1481
Kirby K and Cooper D L 1989 *J. Chem. Phys.* **90** 4895
Klopotek P and Vidal C R 1985 *J. Opt. Soc. Am.* B **2** 869
Klump K N and Lassettre E N 1974 *J. Chem. Phys.* **60** 4830
Kopelman R and Klemperer W 1962 *J. Chem. Phys.* **36** 1693
Krupenie P H 1966 *National Standard Reference Data Series* **5**
Land J E 1978 *J. Appl. Phys.* **49** 5716
Lassettre E N and Skerbele A 1971 *J. Chem. Phys.* **54** 1597
—— 1974 *Methods of Experimental Physics* vol 3b p 868
Mazeau J, Gresteau F, Reinhardt J and Hall R I 1972 *J. Phys. B: At. Mol. Phys.* **5** 1890
Mazeau J, Schermann C and Joyez 1975 *J. Electron Spectrosc. Relat. Phenom.* **7** 269
Middleton A G, Brunger M J and Teubner P J O 1993 *J. Phys. B: At. Mol. Opt. Phys.* **26** 1743
Newman D S, Zubek M and King G C 1983 *J. Phys. B: At. Mol. Phys.* **16** 2247
O'Malley T F 1965 *Phys. Rev.* **137** 1668
Polley J P and Bailey T L 1988 *Phys. Rev.* A **37** 733
Reinhardt J, Joyez G, Mazeau J and Hall R I 1972 *J. Phys. B: At. Mol. Phys.* **5** 1884
Sanche L and Schulz G J 1972 *Phys. Rev.* A **6** 69
Schulz G J 1973 *Rev. Mod. Phys.* **45** 423
Simmons J D and Tilford S G 1974 *J. Mol. Spectrosc.* **49** 167
Skerbele A and Lassettre E N 1974 *J. Chem. Phys.* **55** 424

Skubenich V V 1967 *Opt. Spectrosk.* **23** 540
Sun Q, Winstead C, and McKoy V 1992 *Phys. Rev.* A **46** 6987
Swanson N, Celotta R J, Kuyatt C E and Cooper J W 1975 *J. Chem. Phys.* **62** 4880
Takatsuka K and McKoy V 1984 *Phys. Rev.* A **30** 1734
Trajmar S, Williams W and Cartwright C 1973 *8th Int. Conf. on Physics of Electronic and Atomic Collisions* (Zrenjanin: Grafico Preduzece 'Buducnost') Contributed papers p 349
Viala V P, Letzelter C, Eidelsberg M and Rostas F 1988 *Astron. Astrophys.* **193** 265
Wallbank B, Daviel S, Comer J and Hicks P 1983 *J. Phys. B: At. Mol. Phys.* **16** 3065
Winstead C, Hipes P G, Lima M A P and McKoy V 1991 *J. Chem. Phys.* **94** 5455
Weatherford C A and Huo W M 1990 *Phys. Rev.* A **41** 186
Wolk G L and Rich J W 1983 *J. Chem. Phys.* **79** 12
Zobel J, Mayer U, Jung K and Ehrhardt H 1996 *J. Phys. B: At. Mol. Opt. Phys.* **29**
Zobel J, Mayer U, Jung K, Tripathi D N, Rai D K and Ehrhardt H 1994 *Electron Collisions with Molecules, Clusters and Surfaces* ed H Ehrhardt and L A Morgan (New York: Plenum) p 31